Quantum Electronics **37** (12) 1153 – 1158 (2007)

NONLINEAR OPTICAL PHENOMENA

PACS numbers: 52.50.Jm; 52.38.Hb; 42.65.Re
DOI: 10.1070/QE2007v037n12ABEH013585

Plasma channel localisation during multiple filamentation in air

N.A. Panov, O.G. Kosareva, V.P. Kandidov, N. Aközbek, M. Scalora, S.L. Chin

Abstract. **It is shown by numerical simulations that multiple filamentation of a femtosecond laser pulse with a negative initial phase modulation in air leads to an increase in the density of self-induced laser plasma compared to the case when a transform-limited laser pulse of the same duration is used. Simultaneous control of the duration of the chirped pulse and the beam diameter results in an increase in the distance over which the first filament is formed, the length of the plasma channel, and its linear density.**

Keywords: *plasma channel, femtosecond pulse, filament, lidar*.

1. Introduction

One of the important applications of filamentation [1, 2] of femtosecond subterrawatt and terawatt laser pulses is the remote sensing of the atmosphere because supercontinuum radiation (white light) [3] and fluorescence due to recombination of a plasma in the filament channel [4], which accompany filamentation, carry spectroscopic information on the atmospheric air composition. In the case of remote monitoring based on recording backscattered fluorescence [5], it is extremely important to 'ignite' filaments (i.e., to produce the maximum amount of plasma) at a preset distance from the laser system output. Probing with the help of a supercontinuum calls for increasing the conversion efficiency of laser radiation into white light. When the input pulse energy is fixed, the radiation parameters optimised for producing the maximum plasma density may differ from parameters obtained for the maximum conversion efficiency into supercontinuum [6, 7].

The onset of a filament can be positioned by using various methods. It can be expected that, according to the Marburger formula [8], the increase in the beam diameter with the help of a telescope increases the filament formation distance; however, initial small-scale intensity fluctuations in the beam profile, in which the critical power can be achieved, induce stochastic formation of filaments at distances much shorter than those predicted by the above-mentioned formula. For practical implementation of remote positioning of the filament onset, pulses with a negative initial modulation phase (negative chirp) are used, which experience temporal compression during propagation in a medium with normal dispersion [9, 10].

A detailed numerical simulation of plasma channels and supercontinuum of phase-modulated femtosecond pulses was performed in [11 – 13] in the axially symmetric approximation. The propagation of picosecond chirped pulses with a peak power close to the critical self-focusing power over kilometre-range atmospheric paths was considered in the semianalytic approximation in [14, 15]. As a rule, the formation of a single filament or the absence of filamentation was observed due to the destruction of the transverse beam profile in a turbulent atmosphere. At the same time, the recording of a backscattered fluorescence signal depends on the number of electrons in the plasma channel; consequently, it is most important to produce a bunch of filaments at a preset distance.

For producing a bunch of filaments with a high concentration of the plasma, it was proposed [16, 17] to compress the beam in a telescope by preserving its planar wavefront. For a Ti : sapphire laser emitting 800-nm, 45-fs, 40-mJ pulses, a more than two-orders-of-magnitude increase in the fluorescence signal was observed with decreasing the beam diameter from 25 to 8 mm. The possibilities of this method are limited by the short distance (7 – 10 m) between the beginning of the filament and the laser system output. The idea of producing a filament bunch at a preset distance was developed further in [18], where the telescope mounted at the laser system output served simultaneously for increasing beam diameter and for changing the wavefront curvature. Thus, the beam was first expanded and then focused at a preset distance. The increase in the beam diameter leads simultaneously to an increase in random perturbations and an increase in the distance over which random filaments are formed. In turn, geometrical focusing of the beam 'assembles' filaments at a preset distance. All these factors make it possible to detect nonlinear fluorescence of nitrogen molecules at a distance of up to 92 m. When pulses with negative phase modulation are used, the fluorescence signal increases.

Local measurements showed that the fluorescence signal intensity is determined by the number of free electrons at a

N.A. Panov, O.G. Kosareva, V.P. Kandidov Department of Physics and International Laser Center, M.V. Lomonosov Moscow State University, Vorob'evy gory, 119992 Moscow, Russia; e-mail: panov_na@mail.ru, kosareva@phys.msu.ru, kandidov@phys.msu.ru;
N. Aközbek Time Domain Corporation, 7057 Old Madison Pike, Huntsville, Alabama 35806, USA;
M. Scalora UA Army Aviation and Missile Command, AMSAM-WS-RD-ST, Huntsville, Alabama 35898-5000, USA;
S.L. Chin Centre d'Optique, Photonique et Laser (COPL) et Departement de Physique, de Genie Physique et d'Optique, Universite Laval, Quebec, QC, Canada G1K 7P4

Received 28 March 2007
Kvantovaya Elektronika **37** (12) 1153 – 1158 (2007)
Translated by Ram Wadhwa

preset distance along a filament [7]. Therefore, optimisation of the signal in the case of remote probing based on detecting the backscattered fluorescence is associated with optimisation of the number of free electrons.

The aim of our study is to perform the simultaneous control of a chirped pulse duration and the beam diameter for optimal localisation of the plasma during multiple filamentation in air.

2. Numerical simulation of filamentation of a pulse with initial phase modulation and random perturbations on the beam profile

In the method of slowly varying amplitudes, the propagation of a pulse in air is described by the equation for the electric field envelope $E(x,y,z,t)$:

$$2ik\left(\frac{\partial}{\partial z}+\frac{1}{v_g}\frac{\partial}{\partial t}\right)E=\frac{\partial^2 E}{\partial x^2}+\frac{\partial^2 E}{\partial y^2}-kk''_\omega\frac{\partial^2 E}{\partial t^2}+2k^2\Delta nE$$

$$-ik\left(\alpha^{N_2}+\alpha^{O_2}\right)E, \qquad (1)$$

where v_g is the group velocity; k is the wave number corresponding to wavelength $\lambda=800$ nm; k''_ω is the second-order dispersion coefficient;

$$\alpha^{O_2}=\frac{m^{O_2}\hbar\omega}{I}\frac{\partial N_e^{O_2}}{\partial t},\quad \alpha^{N_2}=\frac{m^{N_2}\hbar\omega}{I}\frac{\partial N_e^{N_2}}{\partial t} \qquad (2)$$

are the parameters characterising multiphoton absorption; $m^{O_2}=8$ and $m^{N_2}=10$ are the numbers of photon required for ionising oxygen and nitrogen molecules in air; and $I=c|E|^2/(8\pi)$ is the radiation intensity. The nonlinear addition to the refractive index is

$$\Delta n=\frac{1}{2}n_2|E|^2-\frac{2\pi e^2 N_e}{m_e\omega^2}, \qquad (3)$$

where the electron concentration N_e in the plasma is the sum of the concentrations of electrons formed due to ionisation of oxygen ($N_e^{O_2}$) and nitrogen ($N_e^{N_2}$),

$$N_e=N_e^{O_2}+N_e^{N_2}; \qquad (4)$$

$n_2=1.6\times10^{-19}$ cm^2 W^{-1} is the Kerr nonlinearity of the medium, which takes into account the inertialess and delayed response and corresponds to a critical power of 6 GW (the increase in the coefficient n_2 during the pulse was neglected because we considered pulse durations exceeding 200 fs); m_e and e are the electron mass and charge, respectively; and ω is the carrier frequency of radiation. The effect of collisions leading to the additional pulse energy loss can be neglected for pulses of duration to $\sim$500 fs.

Electron concentrations $N_e^{O_2}(x,y,z,\tau)$ and $N_e^{N_2}(x,y,z,\tau)$ are calculated from the rate equations for multiphoton ionisation of oxygen and nitrogen:

$$\frac{\partial N_e^{O_2}}{\partial t}=P^{O_2}(I)\left(N_a^{O_2}-N_e^{O_2}\right),$$

$$\frac{\partial N_e^{N_2}}{\partial t}=P^{N_2}(I)\left(N_a^{N_2}-N_e^{N_2}\right), \qquad (5)$$

where ionisation probabilities P^{O_2} and P^{N_2} are determined by using the Perelomov–Popov–Terent'ev model [19] and experimental results [20], and $N_a^{O_2}$ and $N_a^{N_2}$ are the concentrations of neutral oxygen and nitrogen molecules in air.

The initial conditions at the laser system output have the form

$$E(x,y,z=0,\tau)=E_0\exp\left(-\frac{x^2+y^2}{2a_0^2}-\frac{\tau^2}{2\tau_p^2}+i\frac{\delta\tau^2}{2}\right)$$

$$\times[1+\xi(x,y)], \qquad (6)$$

where τ is the running time; $\delta=-\tau_p^2(\tau_p^2/\tau_0^2-1)^{1/2}$; $\tau_0=27$ fs is the transform-limited pulse duration; $\xi(x,y)$ is a two-dimensional random quantity with dispersion $\sigma^2=0.01$ and a correlation radius $r_c=a_0/3$, which is calculated by using the algorithm described in [21]. We considered two values of the beam radius: small ($a_0=1$ mm) and increased ($a_0=1.5$ mm); the duration τ_p of the phase modulated pulse was 200 and 100 fs, respectively. For both cases, the same realisation of random perturbations $\xi(x,y)$ was used. The complex electric field amplitude E_0 in (6) was determined for the total input pulse energy $W_0=24$ mJ.

The second-order dispersion coefficient for air is $k''_\omega=16$ fs^2 m^{-1} at a wavelength of 800 nm; for $\tau_p=100$ fs, the dispersion spread length is $l_{disp}=\tau^2/k''_\omega=625$ m, while the compression length [22] is $l_{comp}=|\delta|\tau_0^2 l_{disp}=162$ m. At the same time, the diffraction length for a beam of radius $a_0=1.5$ mm is $l_{difr}=ka_0^2=17.7$ m. According to the Marburger formula, the self-compression of such a pulse will occur at a distance not exceeding 3 m from the laser system output. Under these conditions, the dispersion effects (first of all, the compression of a pulse with the negative initial phase modulation) will not be manifested. In order to obtain comparable values of the compression length and the self-focusing length, the beam radius should achieve 1 cm. For such a beam radius it is impossible to calculate the plasma density with the help of model (5) because of the phase break due to the steep pulse intensity profile. Because of this, the second-order dispersion coefficient k''_ω was increased to 2000 fs^2 nm^{-1} for numerical simulation of controlling the duration of a pulse with initial phase modulation and the transverse beam size. As a result, the dispersion length l_{disp} decreased to 5 and 20 m for $\tau_p=100$ and 200 fs, respectively. The compression length in these cases was 1.3 and 2.7 m for $\tau_p=100$ and 200 fs respectively, and became comparable with the spatial self-compression length. This made it possible to simulate the space–time control of radiation over long paths in air.

3. Advantages of using pulses with the negative initial phase modulation for producing a plasma channel

In developing laser systems for remote probing and localising of radiation at a preset distance, it is necessary to optimise the output radiation parameters. Based on the results of numerical simulation, we will show that it is often preferable to use pulses with the negative phase modulation than transform-limited pulses of the same duration. Consider the results of two numerical experiments obtained by using model (1)–(5) with initial conditions (6). In the first numerical experiment, the duration of the transform-limited pulse ($\delta=0$) $2\tau_p$ was 400 fs (spectral width $\Delta\lambda\approx4$

nm). In the second numerical experiment, the duration $2\tau_p$ of the chirped pulse was also 400 fs for the spectral width $\Delta\lambda \approx 27$ nm corresponding to the transform-limited pulse duration $2\tau_0 = 54$ fs (or to the 45-fs FWHM). Other initial parameters such as energy $W_0 = 24$ mJ, beam radius $a_0 = 1$ mm, and wavelength $\lambda_0 = 800$ nm were the same in both cases.

Figure 1 shows the transverse radiation intensity distribution at the laser system output in the central layer of the pulse. Note that the peak pulse power proportional to the ratio W_0/τ_p was the same for the transform-limited pulse and the chirped pulse. The chosen radiation parameters correspond to the parameters used in indoor experiments on multiple filamentation of femtosecond laser pulses in air [18]. Due to a decrease in the dispersion length and temporal self-compression length, it is possible to simulate the positioning of plasma on atmospheric paths.

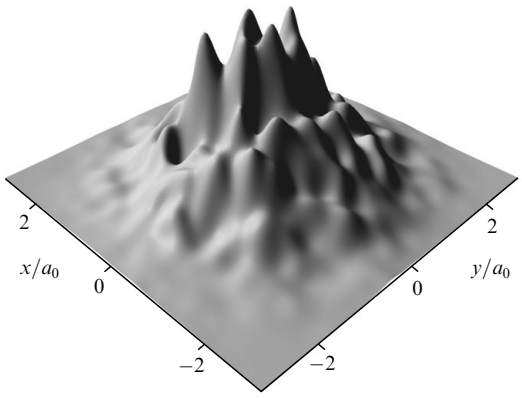

Figure 1. Laser-pulse intensity distribution $I(x, y, \tau = 0, z = 0)$ at the laser system output corresponding to (6). The maximum intensity for $a_0 = 1.0$ and 1.5 mm is the same and equal to 5×10^{12} W cm^{-2}.

Filamentation in the case of transform-limited and chirped pulses of the same duration was analysed by studying the plasma distribution in the beam channel. Free electrons are produced at peak intensities sufficient for multiphoton ionisation of the medium ($\sim 5 \times 10^{13}$ W cm^{-2}). Figure 2 shows plasma channels of filaments, which were determined from a density level of 5×10^{15} cm^{-3}. Figures 2a and 2b correspond to the transform-limited pulse and pulses with the initial phase modulation, respectively. Recall that the density of neutral particles in air is 2.7×10^{19} cm^{-3}.

In the cases of the transform-limited pulse and initially phase-modulated pulse, filaments are formed approximately at the same distance which is determined by self-focusing of small-scale perturbations in the input beam profile (see Fig. 1). The length and number of plasma channels are smaller for the transform-limited pulse (see Figs 2a and 2b).

For a more detailed analysis, we consider the dependence of the linear plasma density D_e (Fig. 3) on the propagation length z. The quantity $D_e(z)$ gives the total number of free electrons formed over distance z

$$D_e(z) = \int N_e(x, y, \tau = \tau_{end}, z)\mathrm{d}x\mathrm{d}y, \qquad (7)$$

where τ_{end} is the instant of time in the coordinate system running with the pulse. By this instant, the pulse intensity

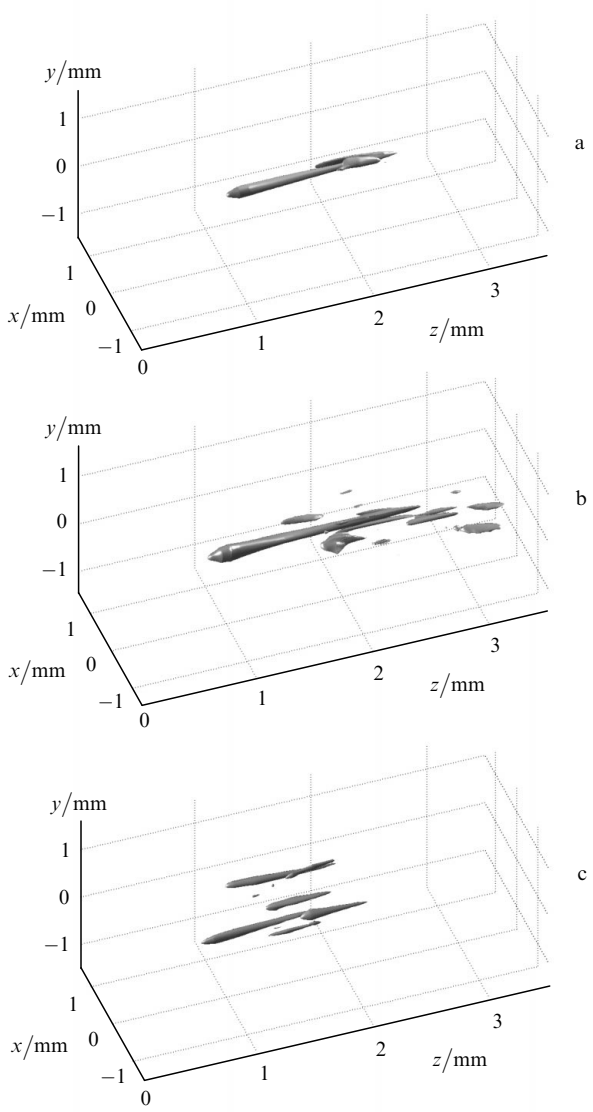

Figure 2. Plasma channels of several filaments for the following cases: (a) transform-limited pulse ($a_0 = 1$ mm, $\tau_p = \tau_0 = 200$ fs); (b) a pulse with a large initial phase modulation and a smaller radius ($a_0 = 1$ mm, $\tau_p = 200$ fs, $\tau_0 = 27$ fs); and (c) a pulse with a large initial phase modulation and a larger radius ($a_0 = 1.5$ mm, $\tau_p = 100$ fs; $\tau_0 = 27$ fs); the longest and the broadest channel corresponds to the case (b).

noticeably decreases and no new free electrons are generated; however, electron–ion recombination has not began. Within the framework of model (1)–(5) neglecting plasma recombination, the value of τ_{end} corresponds to the boundary of the temporal region for calculating radiation conversion. In the transverse region, integration in Eqn (7) is performed over the entire spatial region x, y equal to $8a_0 \times 8a_0$. The solid curve in Fig. 3a shows the dependences $D_e(z)$ for a pulse with the initial phase modulation, while the dashed curve corresponds to the transform-limited pulse.

The first filament in this case is produced almost simultaneously (approximately at a distance of $z = 0.7$ m for the phase-modulated pulse and at a distance of 0.9 m for the transform-limited pulse, Fig. 3a). A later beginning of the filament of the transform-limited pulse is related to its dispersion broadening, while the chirped pulse begins to compress in time immediately after it leaves the laser system. The linear density of the plasma formed during filamenta-

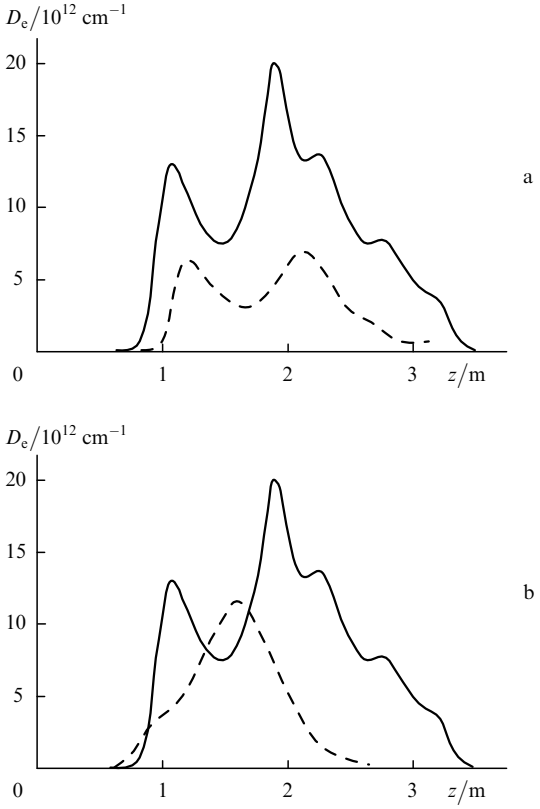

Figure 3. Linear density of the plasma of several filaments for the following cases: (a) transform-limited pulse and a pulse with initial phase modulation [the solid curve corresponds to the phase-modulated pulse ($a_0 = 1$ mm, $\tau_p = 200$ fs; $\tau_0 = 27$ fs, see Fig. 2b), the dashed curve corresponds to a transform-limited pulse ($a_0 = 1$ mm, $\tau_p = \tau_0 = 200$ fs, see Fig. 2a)], and (b) a pulse with initial phase modulation [the solid curve corresponds to a phase-modulated pulse with a smaller radius ($a_0 = 1$ mm, $\tau_p = 200$ fs; $\tau_0 = 27$ fs, see Fig. 2b); the dashed curve corresponds to a phase-modulated pulse of large radius ($a_0 = 1.5$ mm, $\tau_p = 100$ fs; $\tau_0 = 27$ fs, see Fig. 2c)]. The peak values of the linear density of the smaller-radius-pulse plasma are double the corresponding values for a pulse of larger radius.

tion at all points over distance z is higher for the phase-modulated pulse, while the peak values of $D_e(z)$ differ approximately by three times.

Consider the fraction of energy of the input pulse, which is transformed into a self-induced laser plasma,

$$W_e = m^{O_2}\hbar\omega \int D_e^{O_2}(z)dz + m^{N_2}\hbar\omega \int D_e^{N_2}(z)dz, \qquad (8)$$

where $D_e^{O_2}(z)$ and $D_e^{N_2}(z)$ are determined from (7) separately for electrons formed due to ionisation of O_2 and N_2 molecules. In the case of a pulse with the initial phase modulation, the energy in the plasma channels achieves 2.85 mJ, while the energy for the transform-limited pulse is 0.94 mJ (i.e., 11.9 % and 3.9 % of the total pulse energy, respectively). Thus, the conversion efficiency of the radiation energy into the plasma energy for a chirped pulse exceeds this efficiency for the transform-limited pulse approximately by three times. Therefore, the continuous temporal compression of the pulse with the negative phase modulation in a medium with normal dispersion leads to an increase in the intensity and density of the plasma integrated over the beam cross section. Pulses with a negative initial chirp can be recommended for application in laser systems developed for plasma localisation at a certain distance.

4. Joint effect of the negative initial phase modulation and beam diameter on plasma channels in air

The reduction of the beam diameter at the output of a femtosecond laser system leads to multiple (by more than two orders of magnitude) increase in the intensity of the backscattered fluorescence from molecular nitrogen N_2 in the near UV spectral range [18]. At the same time, the first filament is formed during the propagation of the beam with a smaller radius much closer to the output of the laser system as compared to the large-radius beam with the same duration and energy.

To solve this problem, we propose to correct the site of filament nucleation and formation of a plasma channel with the help of the negative initial phase modulation of the pulse. As the chirped-pulse duration is increased, its peak power decreases and the formation of a filament will be delayed. The positioning of the plasma by simultaneous control of the beam diameter and pulse duration was performed by using two numerical experiments. In the first experiment, a relatively large beam radius ($a_0 = 1.5$ mm) and an insignificant phase modulation ($2\tau_p = 200$ fs) were chosen for a transform-limited-pulse duration of $2\tau_0 = 54$ fs. According to the estimate obtained on the basis of the Marburger formula, a filament for such a pulse in the absence of random perturbations in the beam profile should have been formed at a distance $z = 1.79$ m from the output of the laser system. In the second numerical experiment, the beam radius was reduced to 1 mm, while the duration of the chirped pulse was increased to 400 fs. In the absence of random perturbations, the filament should have been formed at a distance $z = 1.25$ m.

The plasma channels obtained as a result of numerical simulation in both cases are shown in Figs 2b and 2c. The beginning of the channels is at approximately the same distance from the laser system outlet ($z \approx 0.7$ m), which differs from the distances estimated using the Marburger formula. In addition, for a small beam radius and a large chirp, the spacing between channels decreases and their length increases.

The linear density of the plasma for $a_0 = 1.0$ mm exceeds that for $a_0 = 1.5$ mm on the entire propagation length except for a small region. The maximal linear density of the self-induced laser plasma is 2.0×10^{13} cm^{-1} for $a_0 = 1.0$ mm and 1.2×10^{13} cm^{-1} for $a_0 = 1.5$ mm. The total energy transformed into plasma energy (8) for $a_0 = 1.5$ mm is 1.18 mJ. In accordance with the estimate obtained in Section 3, this energy is 2.85 mJ for $a_0 = 1.0$ mm (i.e., it amounts to 4.9 % and 11.9 % of the initial energy, respectively). Thus, we obtained a nearly double gain in the maximal linear density and more than double gain in the energy transformed into the plasma energy.

The diameter and relative arrangement of plasma channel are important characteristics in analysis of the quality of plasma source positioning and the backscattered fluorescence intensity. One can see from Figs 2b and 2c that the diameter of the channels for $a_0 = 1.5$ mm is smaller and the spacing between them larger than for $a_0 = 1.0$ mm. Figure 4 shows a detailed pattern of the channels, where the transverse distribution of electron concentration corre-

sponds to distance $z = 1.75$ m both for $a_0 = 1.0$ mm (see Figs 4b and 2b) and for $a_0 = 1.5$ mm (see Figs 4c and 2c). The solid white curve corresponds to the line of equal densities $N_e = 4 \times 10^{15}$ cm^{-3} of free electrons. A plasma formation will be referred to as a filament if electron density N_e in the transverse plane x, y exceeds 4×10^{15} cm^{-3}. For example, we can distinguish four filaments in Fig. 4b and eight filaments in Fig. 4c, the diameter of the latter filament being on the average smaller than the diameter of the filaments shown in Fig. 4b. It can be stated that for the smaller radius ($a_0 = 1.0$ mm) and stronger phase modulation ($2\tau_p = 400$ fs), a bunch of closely spaced filament is formed, while for $a_0 = 1.5$ mm filaments are formed practically independently from one another and with a large spacing.

Let us define the effective diameter of the jth filament as

$$d_j = 2 \times \left\{ \frac{\int N_e(x, y, \tau = \tau_{end}, z)[(x - x_j)^2 + (y - y_j)^2]\mathrm{d}x\mathrm{d}y}{\int N_e(x, y, \tau = \tau_{end}, z)\mathrm{d}x\mathrm{d}y} \right\}^{1/2}, \quad (9)$$

where x_j and y_j are the coordinates of the centre of mass of the filaments described by the expressions

$$x_j = \frac{\int x N_e(x, y, \tau = \tau_{end}, z)\mathrm{d}x\mathrm{d}y}{\int N_e(x, y, \tau = \tau_{end}, z)\mathrm{d}x\mathrm{d}y},$$

$$y_j = \frac{\int y N_e(x, y, \tau = \tau_{end}, z)\mathrm{d}x\mathrm{d}y}{\int N_e(x, y, \tau = \tau_{end}, z)\mathrm{d}x\mathrm{d}y}. \quad (10)$$

Integration in Eqns (9) and (10) is performed over domain x, y, in which the free electron density N_e exceeds 4×10^{15} cm^{-3}. In this case, the mean diameter of the filament can be defined as

$$d = \frac{1}{M} \sum_{j=1}^{M} d_j, \quad (11)$$

where M is the number of filaments. It turns out that at a distance $z = 1.75$ m, the mean diameter is $d = 66$ μm of a filament for the larger-radius input beam ($a_0 = 1.5$ mm) and $d = 99$ μm for the beam with a radius of 1.0 mm. In addition, one can see from Figs 2b, 2c, and 3b that in both cases the plasma is formed at the same distance z and its length for the smaller input beam is more than double the values for the larger input beam.

5. Conclusions

We have discussed the possibility of increasing the density of free electrons in the channels of high-power femtosecond laser pulses in air. Transform-limited and chirped pulses with random initial perturbations of the intensity and phase at the output from the laser system were chosen as the initial pulses. The problem is solved by the method of numerical simulation based on a three-dimensional transient model in space describing diffraction, material dispersion, Kerr self-focusing, and the generation of free electrons in air.

It is shown that femtosecond laser pulses with the negative initial phase modulation are an effective tool for increasing the density and energy of self-induced laser plasma of filaments in comparison with the transform-limited pulses of the same duration. Thus, for an increase in the duration of a transform-limited pulse from 54 to 400 fs after the introduction of the negative initial phase modulation, the maximum linear density of plasma and the energy transformed into the energy of plasma channels were more than doubled.

A simultaneous control of the chirped pulse duration and the transverse beam size makes it possible to check the early formation of plasma channels in the case when beams with a smaller initial diameter are used. A bunch of plasma channels with a lower separation between the centres is formed instead of solitary channels. The duration of plasma formation and the number of free electrons in the channel is doubled upon a simultaneous decrease in the transverse dimensions and an increase in the duration of a pulse with negative phase modulation.

It is intended to optimise further the arrangement and density of plasma channels by broadening the initial beam size to several centimetres followed by geometrical focusing with the help of a telescope [17].

Acknowledgements. This work was supported by the Russian Foundation for Basic Research (Grant Nos 06-

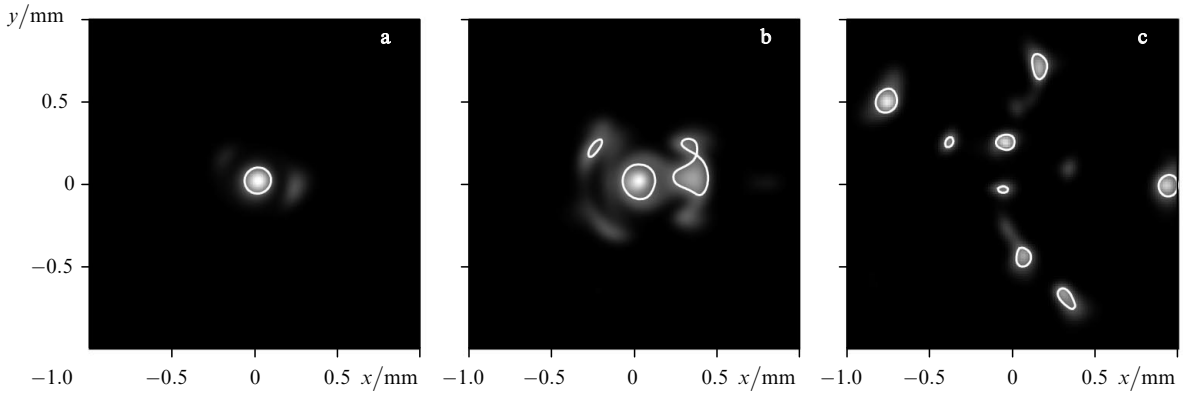

Figure 4. Transverse distribution of electron concentration in plasma channels for the following cases: (a) transform-limited pulse ($a_0 = 1$ mm, $\tau_p = \tau_0 = 200$ fs); (b) a pulse with a small radius and initial phase modulation ($a_0 = 1$ mm, $\tau_p = 200$ fs; $\tau_0 = 27$ fs; a group of closely spaced filaments with a mean diameter of 99 μm is shown); (c) a large-radius pulse with initial phase modulation ($a_0 = 1.5$ mm, $\tau_p = 100$ fs; $\tau_0 = 27$ fs; filaments with a mean diameter of 66 μm are separated by a large distance). The white curve shows the contour with an electron density level in the transverse region of 4×10^{15} cm^{-3}.

02-17508-a and 06-02-08004-ofi), the European Research Office of the US Army (Contract No. W911NF-05-1-0553). The authors thank NATO for support of visits for research purposes (NATO Grant Linkage No. PST.CLG.980383). One of the authors (N.A.P.) thanks the foundation of non-commercial programmes 'Dynasty' for financial support.

References

1. Braun A., Korn G., Liu X., Du D. *Opt. Lett.*, **20**, 73 (1995).
2. Nibbering E.T.J., Curley P.F., Grillon G., Prade B.S., Franco M.A., Salin F., Mysyrowicz A. *Opt. Lett.*, **21**, 62 (1996).
3. Kasparian J., Rodrigues M., Mejean G., Yu J., Salmon E., Wille H., Bourayou R., Frey S., Andre Y.-B., Mysyrowicz A., Sauerbrey R., Wolf J.-P., Wöste L. *Science*, **301**, 61 (2003).
4. Hosseini S.A., Luo Q., Ferland B., Liu W., Chin S.L., Kosareva O.G., Panov N.A., Aközbek N., Kandidov V.P. *Phys. Rev. A*, **70**, 033802 (2004).
5. Luo Q., Liu W., Chin S.L. *Appl. Phys. B*, **76**, 337 (2003).
6. Liu W., Kosareva O.G., Golubtsov I.S., Iwasaki A., Becker A., Kandidov V.P., Chin S.L. *Appl. Phys. B*, **76**, 215 (2003).
7. Deng Y.P., Zhu J.B., Ji Z.G., Liu J.S., Shuai B., Li R.X., Xu Z.Z., Théberge F., Chin S.L. *Opt. Lett.*, **31**, 546 (2006).
8. Marburger J.H. *Prog. Quantum Electron.*, **4**, 35 (1975).
9. Wille H., Rodrigues M., Kasparian J., Mondelain D., Yu J., Mysyrowicz A., Sauerbrey R., Wolf J.P., Woste L. *Eur. Phys. J. Appl. Phys.*, **20**, 183 (2002).
10. Rodrigues M., Bourayou R., Mejean G., Kasparian J., Yu J., Salmon E., Scholz A., Stecklum B., Eislöffel J., Hatzes P.A., Sauerbrey R., Wöste L., Wolf J.-P. *Phys. Rev. E*, **69**, 036607 (2004).
11. Golubtsov I.S., Kandidov V.P., Kosareva O.G. *Kvantovaya Elektron.*, **33**, 525 (2003) [*Quantum Electron.*, **33**, 525 (2003)].
12. Kandidov V.P., Golubtsov I.S., Kosareva O.G. *Kvantovaya Elektron.*, **34**, 348 (2004) [*Quantum Electron.*, **34**, 348 (2004)].
13. Nuter R., Skupin S., Bergé L. *Opt. Lett.*, **30**, 917 (2005).
14. Peano J.R., Sprangle P., Hafizi B., Ting A., Gordon D.F., Kapetanakos C.A. *Phys. Plasmas*, **11**, 2865 (2004).
15. Shlenov S.A., Fedorov V.Yu., Kandidov V.P. *Opt. Atmos. Okean.*, **20**, 308 (2007).
16. Luo Q., Hosseini S.A., Liu W., Gravel J.-F., Kosareva O.G., Panov N.A., Aközbek N., Kandidov V.P., Roy G., Chin S.L. *Appl. Phys. B*, **80**, 35 (2004).
17. Kosareva O.G., Panov N.A., Aközbek N., Kandidov V.P., Luo Q., Hosseini S.A., Liu W., Gravel J.-F., Roy G., Chin S.L. *Appl. Phys. B*, **82**, 111 (2005).
18. Liu W., Théberge F., Daigle J.-F., Simard P.T., Sarifi S.M., Kamali Y., Xu X.L., Chin S.L. *Appl. Phys. B*, **85**, 55 (2006).
19. Perelomov A.M., Popov V.S., Terent'ev M.V. *Zh. Eksp. Teor. Fiz.*, **50**, 1393 (1966).
20. Talebpour A., Yang J., Chin S.L. *Opt. Commun.*, **163**, 29 (1999).
21. Mirkin L.I., Rabinovich M.A., Yaroslavskii L.P. *Vychisl. Matem. Mat. Fiz.*, **12**, 1353 (1972).
22. Akhmanov S.A., Vysloukh V.A., Chirkin A.S. *Optika femtosekundnykh lazernykh impulsov* (Optics of Femtosecond Laser Pulses) (Moscow: Nauka, 1988).